ELSEVIER

Effects of Sun and View Geometries on Cotton Bidirectional Reflectance. Test of a Geometrical Model

M. Verbrugghe[*] *and J. Cierniewski*[†]

During the MAC-VI campaign, bidirectional reflectance measurements were taken on a cotton crop in order to analyze the effects of sun and view geometries in the wavebands and in the viewing vertical plane of the SPOT High Resolution Visible (HRV) instrument. The bidirectional reflectance was measured using a CIMEL SPOT simulation radiometer fixed on a goniometric apparatus 2 m above the top of the crop. Data are presented in terms of bidirectional reflectance factors relative to nadir reflectance for 15 view angles (−70° to +70°) and for 12 solar zenith (73–26°) angles. Results show major variations according to Sun position and backscattering or forward scattering observations. The relative reflectance factor of the cotton varies from 0.7 to 1.9 throughout one day. Measurements are compared to the output of a geometrical model where cotton rows are simulated by spheroidal cylinders sitting on an horizontal surface. The relative reflectance factor is calculated according to the global structure of the rows which is divided into illuminated and shaded facets viewed by the radiometer for each view and solar angle. The analysis of comparative results shows a good agreement between predicted and measured data in the three SPOT HRV wavebands.

INTRODUCTION

Natural surfaces are generally non-Lambertian and the analysis of their spectral properties with ground, aircraft, or satellite remote sensing data is dependent on view and sun angles (Huete et al., 1992; Jackson et al., 1990; Jasinski, 1990; Moran et al., 1990; Pinter et al., 1990; Royer et al., 1985; Guyot, 1984; Kimes et al., 1984; Slater and Jackson, 1982). It is, therefore, necessary to take into account the bidirectional reflectance distribution function (BRDF) of the target to compare quantitatively the measurements acquired under different illumination and observation conditions. Knowledge of the bidirectional properties of natural surfaces is particularly important for correcting images acquired by satellites with wide-angle imagery sensors such as the Advanced Very High Resolution Radiometer (AVHRR) on board NOAA satellites or with variable view angle sensors such as the High Resolution Visible instrument (HRV) on board SPOT satellites. Empirical corrections on bidirectional effects are easier when variable view angle sensors include, at the same time and for exactly the same surface, off-nadir, and nadir views. This approach is, for instance, possible for the Advanced Solid-State Array Spectroradiometer (ASAS) or for the Along Track Scanning Radiometer (ATSR) of the European Remote Sensing Satellite (ERS1).

The aim of this article is to present the bidirectional reflectance properties of a cotton crop made at ground level, in SPOT (HRV) spectral bands and view plane. The first part of this article presents the experimental results, and then these results are compared in the second part to the output of a geometrical model which takes into account the effects of Sun and view geometries on crop bidirectional reflectance.

MATERIALS AND METHODS

The experiment was conducted at the University of Arizona's Maricopa Agricultural Center (MAC) near Phoenix, Arizona, during the MAC-VI experiment (7 and 8 September 1991). The measurements were made in a furrowed field of cotton (*Gossypium hirsutum*). The

[*]INRA Bioclimatologie, Montfavet, France
[†]Institute of Physical Geography, Adam Mickiewicz University, Poznan, Poland

Address correspondence to Verbrugghe, INRA Bioclimatologie, Domaine Saint Paul, Site Agropare, 84914 Avignon Cedex 9, France.
Received 27 June 1994; revised 19 July 1995.

REMOTE SENS. ENVIRON. 54:189–197 (1995)

655 Avenue of the Americas, New York, NY 10010

0034-4257/95/$9.50
SSDI 0034-4257(95)00174-Y

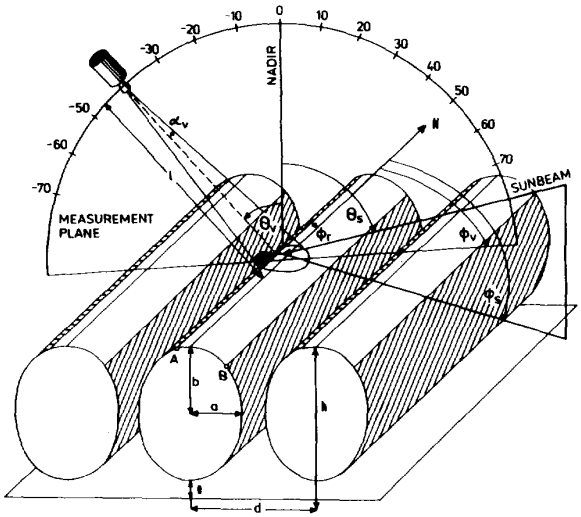

Figure 1. Schema of the model representation and its parameters.

rows were oriented in the north–south direction, and spaced 1 m apart. The height of the vegetation from the top of the furrow was 1.03 m and the cotton canopy cover was about 85%.

The bidirectional reflectance factor (BRF) of a cotton canopy was measured, with a CIMEL SPOT HRV simulation radiometer (with HRV equivalent spectral bands of 500–590 nm, 615–680 nm, and 790–890 nm) fixed on a tubular goniometric support. The radiometer measured the BRF in the view plane of the SPOT HRV instrument (approximately 100° N with 10°view angle increment variations, from − 70° to + 70° (Fig. 1). The radiometer was at 1.9 m above the target center (top of the crop), and it was moved along an arc centered on the middle of the cotton row. With the field-of-view (FOV) of 12° of the CIMEL radiometer, the spatial resolution at nadir viewing was 0.40 m in diameter at the top of the canopy. The measurements were taken all day long, about every 30 min, and the solar zenith angles varied from 73° to 26°. For each sun position the nadir measurement was taken as the reference value at the beginning, in the middle and at the end of each sequence, which lasted about 5 min, for 17 view angles. The data were recorded on a CIMEL datalogger. The relative reflectance factor for each band was obtained by computing the ratio between the output signal of the radiometer in off-nadir and those in nadir measurement, the latter being, for each sequence, the mean value of the three nadir measurements.

The results are presented in terms of the relative bidirectional reflectance factor (RBRF) (the ratio between off-nadir and nadir reflectance factors). Negative view angles correspond to forward scattering measurements and positive angles to backscattering measurements. The view and sun angle effects on RBRF are shown in Figure 2. The variations of the RBRF with view and sun angles had similar patterns in the three spectral bands. Nevertheless, the variations were less pronounced in the near infrared (XS3) than in visible bands (XS1 and XS2) especially for angles greater than 40°. This can be explained by the transmittance and absorptance properties of the cotton crop. Vegetation is more transparent in the near-infrared than in the visible spectral bands, and, therefore, the shadow and angle effects on NIR are smaller than on visible channels. The variations of the relative reflectance factor increased with an increase in solar zenith angle. The angular effects were more pronounced for high solar zenith angles and in the backscattering observations. The extreme values of the RBRF varied from 0.7 to 1.9 in visible and 0.7 to 1.45 in the infrared spectral bands. For the extreme view angles of SPOT (− 30° to + 30°), variations of the RBRF of 0.8 to 1.2 in the visible and of 0.8 to 1.12 in the infrared were observed. These results have to be taken into account in all calculations of relationships between crops and radiations as for example in vegetation index calculation or in oblique imagery analysis (Jackson et al., 1990).

Bidirectional effects have to be taken into account to calculate vegetation indices. Figure 3 shows, for instance, the variations during half a day of the near-infrared and red ratio (NIR/red), in relation to the solar zenith angle and the view angle. The results are presented in terms of the values relative to the NIR/Red ratio measured at noon. The values of this relative ratio were largely dependent on the geometric condition of measurements. The extreme differences was 22% for nadir viewing observations when solar zenithal angle varied from 26° to 73°. The difference was about 40% between + 60° and − 60° view angles for a 73° solar zenithal angle.

The relative importance of the illuminated and shaded surfaces and the effects of the slopes and the orientations of these surfaces viewed by the radiometer can explain these results. The analysis of these directional properties of cotton will be specified in the second part of this article by the modeling.

A GEOMETRIC BIDIRECTIONAL REFLECTANCE MODEL

Modeling the bidirectional reflectance of natural land surfaces was undertaken essentially by radiative transfer models (Pinty and Verstraete, 1992; Goel and Reynolds, 1989; Hapke, 1984) or by geometrical models (Irons et al., 1992; Deering et al., 1989; Cierniewski, 1987). To predict the bidirectional reflectance distribution of a cotton canopy in visible and reflective infrared wavebands, a geometric model was developed in this study. It is based on the concept of a vegetation surface repre-

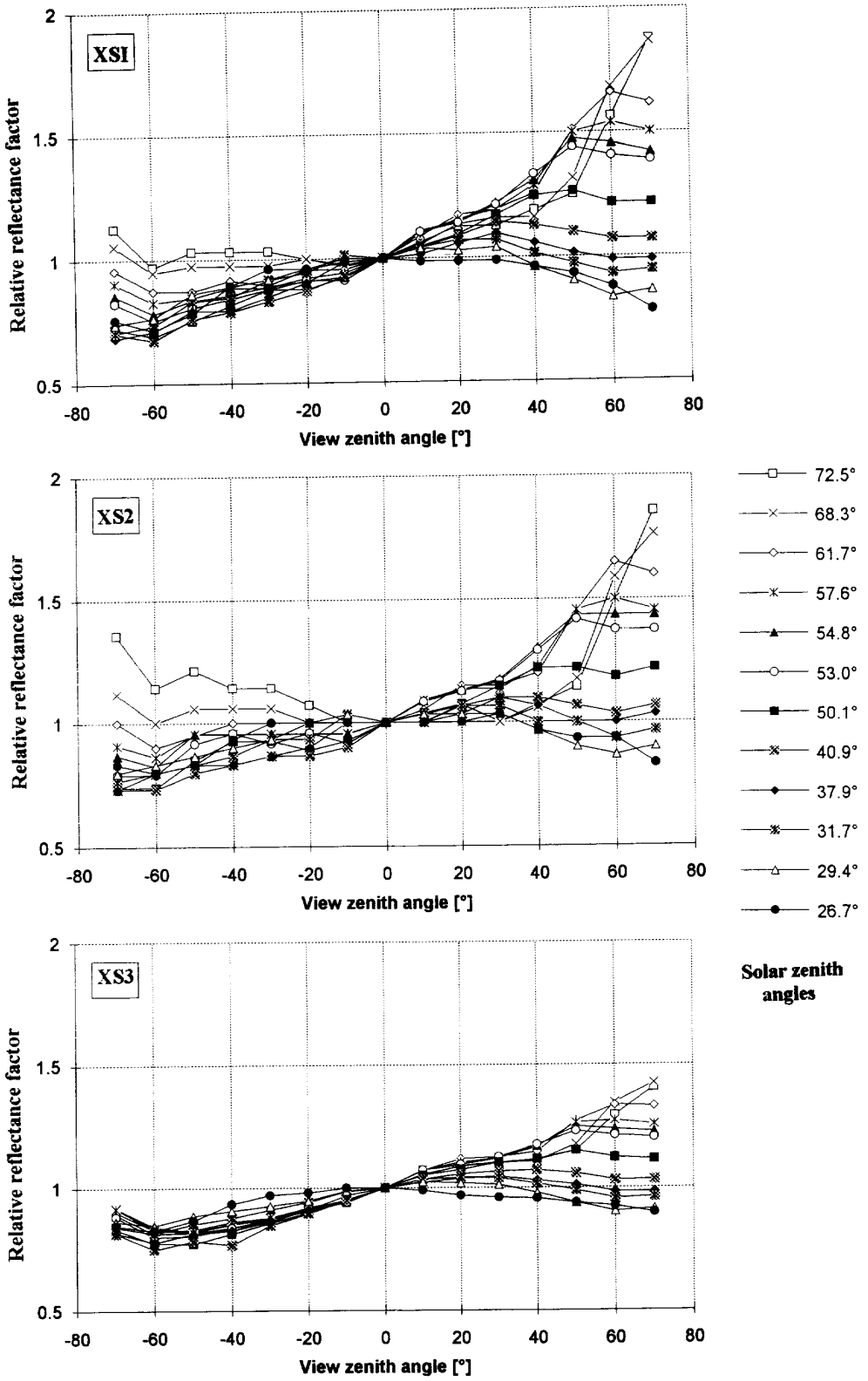

Figure 2. Measured relative reflectance factors of a cotton canopy for the three SPOT bands (XS1, XS2, XS3) along SPOT viewing plane. Negative view angles correspond to forward scattering directions, positive angle to backscattering directions. The different curves correspond to different solar zenith (SZA) and azimuth (SAA) angles.

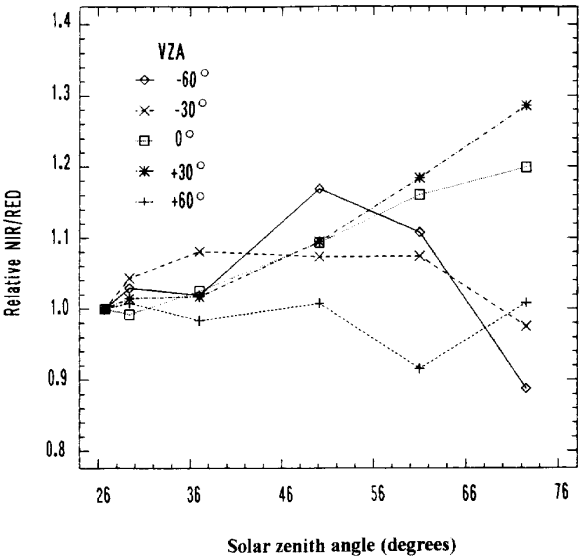

Figure 3. Variations of the relative ratio NIR / R along SPOT plane versus view zenith (VZA) angles and solar zenith angles.

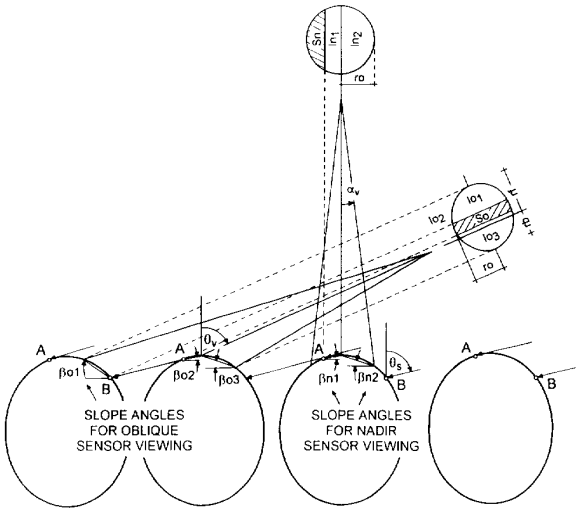

Figure 4. Geometrical determination of slopes, and shaded and illuminated facets.

sented by a collection of opaque spheroidal cylinders placed at a height (e) over a horizontal plane (Fig. 1). The cylinders, simulating plant rows, are characterized by their horizontal (a) and vertical (b) radii. The rows are parallel and (d) is the distance between rows center. The angle φ_r is the azimuth angle of the rows with respect to the north, and h is the total height of the plant rows above the soil. The geometrical structure is illuminated by sunbeams having a zenith angle θ_s and an azimuth angle φ_s, and the nadir view position of the radiometer is exactly over the center of one row, at a distance (l) from its top. The angles θ_v and φ_v, respectively, describe the zenithal and azimuthal position of the radiometer. The FOV of the radiometer is α_v.

The model first calculates the areas of the different facets of illuminated surface in oblique I_o or nadir I_n view, and the areas of different shaded facet for oblique S_o and nadir view S_n (Fig. 4). The facets are defined by the limits of sunlit and shaded surfaces, the top of the row, the FOV of the radiometer and the radiometer's distance from each facet. For oblique observations, the target viewed by the radiometer is not a circle but a deformed ellipse defined by the radii r_b and r_f, which are determined by the top of the row and the limits of the surface. The points positioning the limit between the sunlit and shaded fragments are determined analytically by solving trigonometrical equations. The coordinate system originates at the top of the row above which the radiometer is at its zenith position. For the vegetation surfaces, these points are calculated as tangential points A (Fig. 4) between the simulated sunbeams and the canopy surface, and as the intersection points B of the sunbeams with the vegetation rows. The A and B positions in the plane radiometer FOV, obliquely looking at the vegetation with the θ_v angle, are calculated as for the rotated coordinate system of the θ_v angle. The model takes into account in the FOV sunlit and shaded fragments of the given cylinder, the adjoining cylinders, and the soil surface between the cylinders.

Table 1. Correlation Coefficient (r), Root Mean Square (rms), and Parameters of the Linear Regression Equation Slope and Intercepted (int) between the Measured and Predicted data for the Ellipse and Deformed Spheroidal Cotton Rows for the Three Spectral Bands of the SPOT HRV (XS1, XS2, and XS3)

	Ellipse				*Deformed Ellipse*			
Channel	*r*	*rms*	*Slope*	*int*	*r*	*rms*	*Slope*	*int*
XS1	0.821	0.100	0.674	0.329	0.922	0.088	0.979	0.046
XS2	0.815	0.102	0.797	0.197	0.898	0.100	1.137	−0.124
XS3	0.807	0.104	1.056	−0.03	0.904	0.097	1.532	−0.475

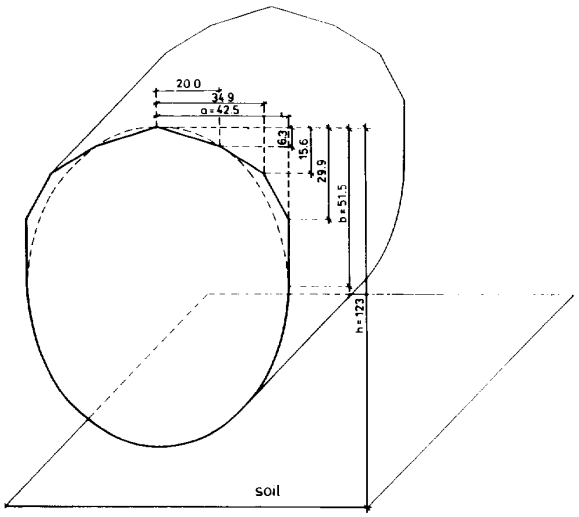

Figure 5. Schema of the deformed ellipse.

The model divides curvilinear slopes of the sunlit vegetation fragments into simple linear subslopes of the angles β_i. These angles, together with the azimuth position of the slopes, φ_r, and sun zenith angle θ_s and sun azimuth angle φ_s, determine the amount of energy reaching these sunlit surfaces using the factor E_{β_i} defined as

$$E_{\beta_i} = \cos\theta_s \cos\beta_i + \sin\beta_i \sin\theta_s (\sin\varphi_s \sin\varphi_r + \cos\varphi_s \cos\varphi_r).$$

The factor E_{β_i} takes the value 1 when the sunbeams reach perpendicular position to the analyzed surface and the value 0 when the sunbeams are tangent to a given surface. Negative values of this factor mean that the surface is shaded. Assuming that energy reflected by each facet is directly proportional to E_{β_i} and that energy reflected by shaded fragments has an isotropic distribution, we can define a factor of proportionality of radiance L for a given view and Sun geometry and a given wavelength by the expression

$$L = \frac{\sum_{i=1}^{j} (E_{\beta_i} I_i).(1-f) + S \cdot f}{\sum_{i=1}^{j} I_i + S},$$

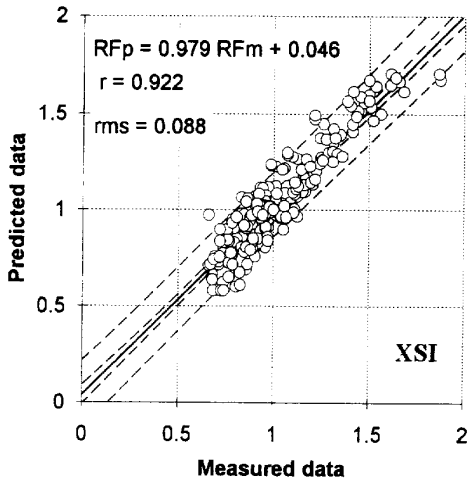

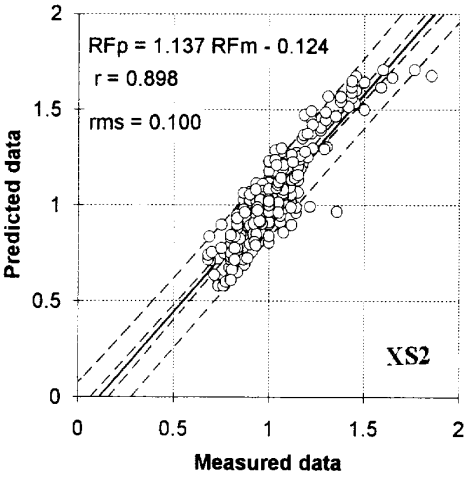

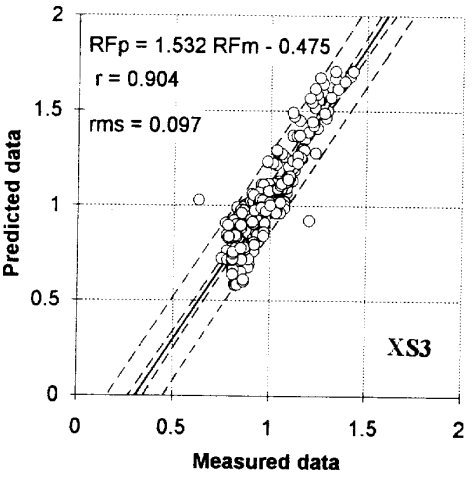

Figure 6. Comparisons between predicted and measured data for XS1, XS2, and XS3 and for all the available data (300 points). The 90% and 95% confidence interval are also plotted.

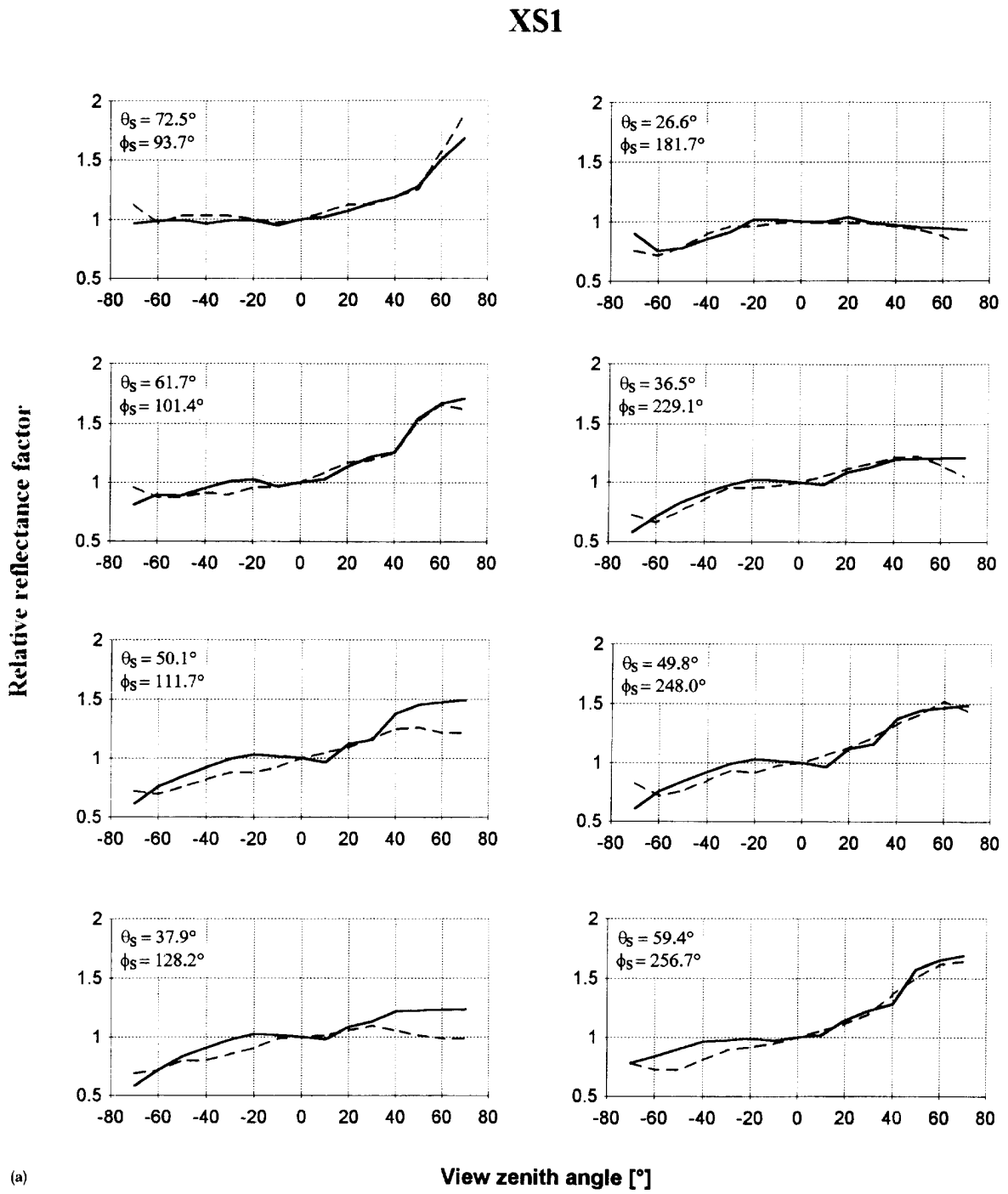

Figure 7. Comparisons of the variations of predicted (— — —) and measured (. . .) relative reflectance factors for (a) a visible (XS1) and (b) an infrared (XS3) band along SPOT plane versus view angles for several sun positions.

(*Continued*)

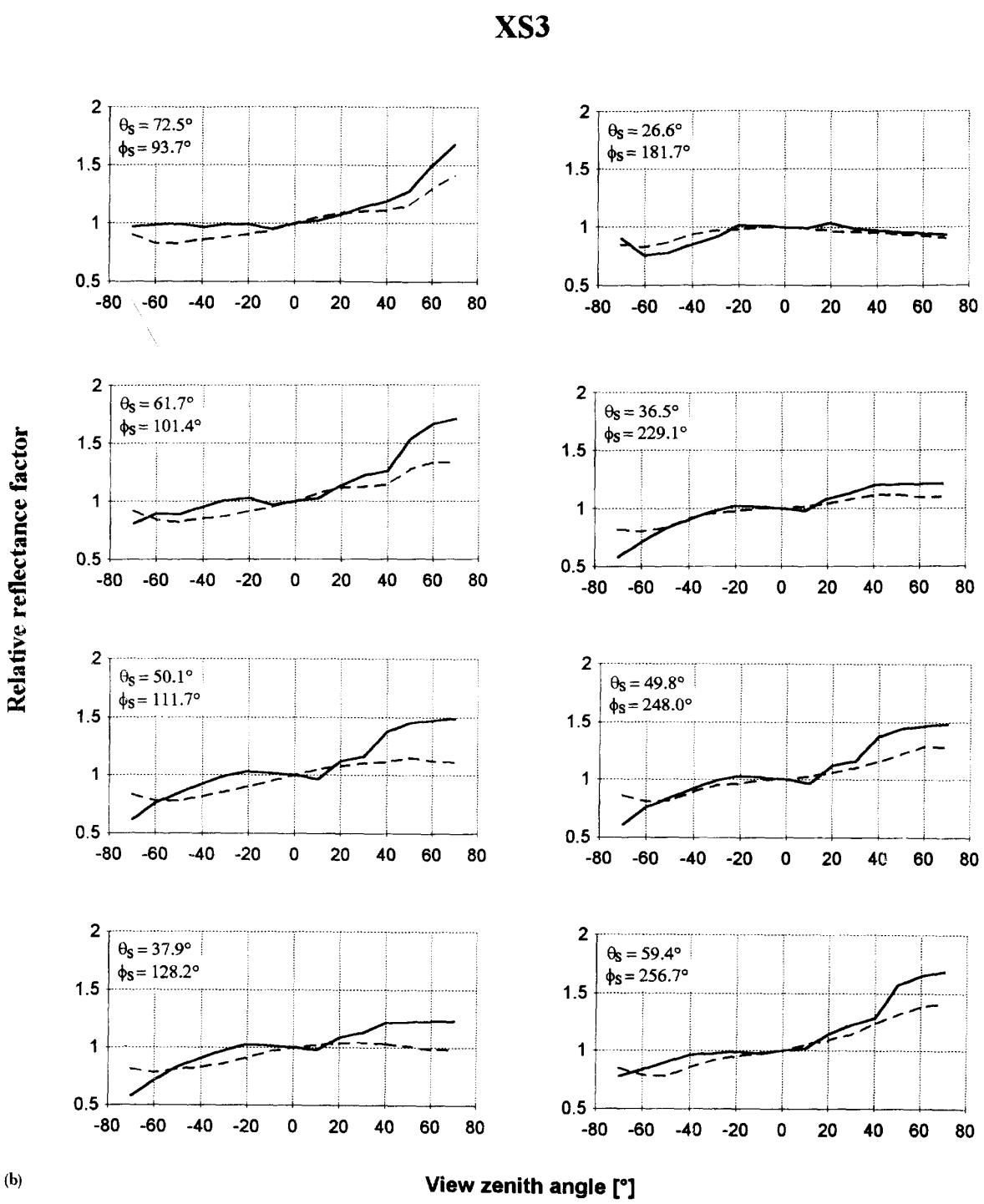
XS3
θs = 72.5°
φs = 93.7°
θs = 26.6°
φs = 181.7°
θs = 61.7°
φs = 101.4°
θs = 36.5°
φs = 229.1°
θs = 50.1°
φs = 111.7°
θs = 49.8°
φs = 248.0°
θs = 37.9°
φs = 128.2°
θs = 59.4°
φs = 256.7°
Relative reflectance factor
View zenith angle [°]
(b)

where

I_i = area of the illuminated facet i,
S = area of the shaded fragment,
j = number of facets,
f = fraction of the diffuse radiation (ratio between radiance of a shaded surface and radiance of the same surface but sunlit).

The fraction f was selected by choosing the value that results the lowest root mean square and the highest correlation coefficient between the model output and the measured data. The f coefficient obtained this way equals 0.33 for the three wavebands. The relative reflectance factor of the target is defined as the ratio between the factors of proportionality of radiances in off-nadir view (L_s) and in nadir view (L_o):

$$\mathrm{RF} = \frac{L_s}{L_o}.$$

In the first step, the bidirectional reflectance distribution of the cotton field was predicted by the model using the following input data:

$a = 42$ cm, $b = 51.5$ cm, $d = 100$ cm,
$h = 123$ cm, $1 = 200$ cm, $\varphi_r = 0°$,
$\varphi_v = 102°$, $a_v = 6°$.

In the second step, the ellipsoidal shape was deformed in order to describe more precisely the shape of the cotton rows in a plane perpendicular to their long axis. Simplifying the curvilinear row slope with straight lines as in Figure 5 made it easier to calculate specific points defining the range of the sunlit and shaded fragments of the surface visible by the sensor.

Statistical parameters describing regression analysis between all the measured (300 data points) and simulated data for an ideal or a deformed ellipse are presented in Table 1. These results show that if the coefficients of determination r are 0.82, 0.81, and 0.81 for XS1, XS2, and XS3 in the case of an ideal ellipse, the deformed ellipse greatly improves the performance of the model. In the case of the deformed ellipse the r coefficient is about 0.90, and the root mean square about 0.10 in the three channels. We also note that the slopes are close to 1 and the intercept close to 0 for the channels XS1 and XS2. For the channel XS3, the transmittance properties which are not taken into account by the model could be the cause of the deviation from 1 for the slope and 0 for the intercept. These results are illustrated in Figure 6 which presents the linear regression between the predicted and the measured data obtained with the deformed ellipse.

In Figures 7a and 7b, we compare in detail the variations of predicted and measured reflectance factors in the visible band (XS1) and in the infrared band (XS3) in relation with view zenith angles at different solar zenith and solar azimuth angles throughout one day. The shapes of the curves are similar. The agreement between modeled and measured reflectance factors is especially good in the visible channel. In the infrared we observe some discrepancies for view angles greater than 40° in backscattering direction. This is due to the transmittance properties of the vegetation in this waveband. If we consider the comparison only inside the extreme view angles of the SPOT HRV (−30° to +30°), we observe that the model performs reasonably well in visible (XS1) and near-infrared (XS3) wavelengths.

CONCLUDING REMARKS

The results show the importance of view and Sun geometry effects on bidirectional reflectance factor of cotton. It is necessary to take into account the directional effects of such a surface to quantitatively compare reflectance data of different measurement conditions. The observed differences of reflectance factor can lead to major errors in remote sensing data interpretations. The results presented in this article show that, in the view plane of the SPOT HRV, the relative BRF vary from 0.7 to 1.9 in the visible range throughout the day due to view and Sun angle geometry. The non-Lambertian properties of the vegetation surface are more pronounced as the Sun and view zenith angles increase.

The geometric model proposed in this article takes into account the general shape of the cotton rows and the geometry of each illuminated and shaded facet viewed by the radiometer. The correlations between the measured and predicted data are reasonably good and can help to correct remote sensing data from directional effects. These preliminary results need to validated with data from other experiments which address soil surface effects and crop architectures.

The authors wish to thank Odile Taconet (CRPE, Velisy) for her very helpful contribution in acquiring measurements and Ray Jackson, Susan Moran, and Tom Clarke (USDA, Phoenix, Arizona) for their welcome and help during the MAC-VI experiment.

REFERENCES

Cierniewski, J. (1987), A model for soil surface roughness influence on the spectral response of bare soils in the visible and near-infrared range, *Remote Sens. Environ.* 23: 97–115.

Deering, D. W., Eck, T. F., and Otterman, J. (1989), Bidirectional reflectances of three soils surfaces and their characterization through model inversion, in *Proc. of the 1989 Int. Geosciences and Remote Sensing Symposium (IGARSS' 89) and the Twelfth Canadian Symposium on Remote Sensing*, Vancouver, BC, pp. 670–673.

Goel, N. S., and Reynolds, N. E. (1989), Bidirectional canopy reflectance and its relationship to vegetation characteristics, *Int. J. Remote Sens.* 10:107–132.

Guyot, G. (1984), Variabilité angulaire et spatiale des données spectrales dans le visible et le proche infrarouge, in *Proc. IIe Coll. Int. Signatures Spectrales d'Objets en Télédétection, Les Colloques de l'INRA n° 23, Bordeaux Ed.INRA*, pp. 27–44.

Hapke, B. (1984), Bidirectional reflectance spectroscopy, *Icarus* 59:41–59.

Huete, A. R., Hua, G., Qi, J., Chebouni, A., and Van Leeuwen, W. J. D. (1992), Normalization of multidirectional red and NIR reflectances with the SAVI, *Remote Sens. Environ.* 41: 143–154.

Irons, J. R., Campbell, G. S., Norman, J. M., Graham, D. W., and Kovalick, W. M. (1992), Prediction and measurement of soil bidirectional reflectance, *IEEE Trans. Geosci. Remote Sens.* 30:249–259.

Jackson, R. D., Teillet, P. M., Slater, P. N., et al. (1990), Bidirectional measurements of surface reflectance for view angles correction of oblique imagery, *Remote Sens. Environ.* 32: 189–202.

Jasinski, M. (1990), Sensitivity of normalized difference vegetation index to subpixel canopy cover, soil albedo, and pixel scale, *Remote Sens. Environ.* 32:169–187.

Kimes, D. S., Newcomb, W. W., Schutt, J. B., Pinter, P. J., Jr., and Jackson, R. D. (1984), Directional reflectance factor distributions of a cotton row crop, *Int. J. Remote Sens.* 5: 263–277.

Moran, M. S., Jackson, R. D., Hart, G. F., et al. (1990), Obtaining surface reflectance factors from atmospheric and view angle corrected SPOT-1 HRV data, *Remote Sens. Environ.* 32:203–214.

Pinter, P. J., Jr., Jackson, R. D., and Moran, M. S. (1990), Bidirectional reflectance factors of agricultural targets a comparison of ground- aircraft, and satellite-based observations, *Remote Sens. Environ.* 32:215–228.

Pinty, B., and Verstraete, M. (1992), On the design and validation of surface bidirectional reflectance and albedo models, *Remote Sens. Environ.* 41:155–167.

Royer, A., Vincent, P., and Bonn, F. (1985), Evaluation and correction of viewing angles effects on satellite measurements of bidirectional reflectance, *Photogramm. Eng. Remote Sens.* 51:1899–1914.

Slater, P. N., and Jackson, R. D. (1982), Atmospheric effects on radiation reflected from soil and vegetation as measured by orbital sensors using various scanning directions, *Appl. Opt.* 21:3923–3931.